JBIC Journal of Biological Inorganic Chemistry (2019) 24:53–60
https://doi.org/10.1007/s00775-018-1626-9

ORIGINAL PAPER

Metalloporphyrin–indomethacin conjugates as new photosensitizers for photodynamic therapy

Fengshou Wu[1] · Mengqian Yang[1] · Juan Zhang[2] · Sizhe Zhu[1] · Mengge Shi[1] · Kai Wang[3]

Received: 10 July 2018 / Accepted: 8 October 2018 / Published online: 22 October 2018

Abstract
Photodynamic therapy (PDT) is a promising cancer treatment approach with the advantages of low toxicity and noninvasive characteristics. In this study, a series of metalloporphyrin–indomethacin conjugates tethered with poly(ethylene glycol) (PEG) chains were prepared and characterized. The singlet oxygen production of the conjugates was evaluated through 2′, 7′-dichlorofluorescin (DCFH) method. Because of the heavy atom effect, the metal porphyrin complexes exhibited the higher singlet oxygen ($^1O_2$) quantum yield than that of free base porphyrin. The order of $^1O_2$ yield of the synthesized porphyrins was PtPor > PdPor > ZnPor > Por. The MTT assay using HeLa cells verified the low cytotoxicity of porphyrin–indomethacin conjugates in the dark. Upon irradiation, the platinated porphyrin (PtPor) showed the highest therapeutic activity among these conjugates, probably due to its high efficiency of $^1O_2$ generation. The cellular uptake and subcellular localization of the conjugates were further evaluated through a confocal laser scanning microscope. The results showed that the conjugates were primarily localized in the lysosomes of HeLa cells.

Keywords Porphyrin · Heavy metal · Biocompatibility · Photosensitizers · PDT

Introduction

Cancer has become the major threat to human beings' wellness around the world over the past two decades, and considerable efforts have been devoted to the cancer treatment. Photodynamic therapy (PDT) is a minimal invasive therapy that has been clinically approved for the cancer treatment with selective cell toxicity [1–3]. In photodynamic therapy, photosensitizers (PSs) are irradiated by a specific wavelength of light, which triggers the generation of reactive oxygen species from intracellular oxygen that consequently induce cell death and necrosis of proximal tissues [4, 5]. Thus, the photosensitizer is the key factor for PDT, which usually requires high ROS generation yield, and good water solubility and biocompatibility. The most commonly used PSs are porphyrin-based molecules. Some of them have been approved by the multinational governments drug regulatory authorities and were widely applied in clinic due to their strong photosensitizing effect, low toxicity and low side effects to the human body [6, 7]. However, many of the porphyrin derivates are limited because of poor water solubility, low bioavailability and no specific targeting to tumors [8, 9]. Therefore, rational design of porphyrin-based photosensitizers with good biocompatibility and high singlet oxygen quantum yield (QY) is very desirable for photodynamic cancer therapy [10].

Polyethylene glycol (PEG) is a hydrophilic and biocompatible polymer chain, which showed little toxicity, and is easily eliminated from the body intact by either the kidneys (for PEG < 30 kDa) or in the feces (for PEG > 20 kDa) [11]. It is approved by FDA for use as a carrier for foods, cosmetics and pharmaceuticals or base [12]. In 2016, Huang et al. reported that the modification of photosensitizer with

✉ Fengshou Wu
wfs42@126.com

✉ Kai Wang
kaiwang@hubu.edu.cn

1 Key Laboratory for Green Chemical Process of the Ministry of Education, School of Chemical Engineering and Pharmacy, Wuhan Institute of Technology, Wuhan, People's Republic of China

2 School of Chemistry and Environmental Engineering, Wuhan Institute of Technology, Wuhan, People's Republic of China

3 Hubei Collaborative Innovation Center for Advanced Organic Chemical Materials, College of Chemistry and Chemical Engineering, Hubei University, Wuhan, People's Republic of China

polyethylene glycol (PEG) could modulate its pharmacokinetic properties [13]. Besides, the PEGylation of medicine allows it to pass through the vascular wall conveniently to accumulate in tumor tissue, and stay in tumor tissue for a long time without being cleared up by lymphatic reflux [10]. Thus, the porphyrin compounds functionalized with polyethylene glycol (PEG) chains could significantly improve their solubility and biocompatibility.

On the other hand, to enhance the active targeting of photosensitizers, a common strategy is a direct conjugation of drugs with targeting ligands, such as monoclonal antibodies, proteins, peptides, and other small molecules [14]. Indomethacin (INDO), as one of the first non-steroidal anti-inflammatory drugs (NSAID), has been widely used in the treatment of inflammatory diseases [15, 16], such as rheumatoid arthritis, osteoarthritis, gut arthritis, burst, tendinitis, traumatic synovitis, and ankylosing spondylitis. The previous reports have verified that indomethacin has antitumour activity and its conjugates could bind tightly and selectively to cyclooxygenase-2 (COX-2), which is expressed in only a few normal tissues, but is found at high levels in inflamed tissues and many premalignant and malignant tumors [17].

In this context, here we designed and synthesized a new porphyrin–indomethacin conjugate tethered with poly(ethylene glycol) (PEG) chains. Since the heavy metal ions could enhance the intersystem crossing, which in turn improves the capacity of singlet oxygen generation [18, 19], the synthesized porphyrin–indomethacin conjugate was further coordinated with Zn, Pd and Pt, respectively, to yield three new photosensitizers (ZnPor, PdPor and PtPor). As expected, the platinated porphyrin (PtPor) displayed the highest singlet oxygen quantum yield among these four photosensitizers. Finally, the cytotoxicity and subcellular localization of the porphyrin–indomethacin conjugates were further evaluated through MTT method and confocal laser scanning microscope, respectively.

Experiment sections

General

All chemicals were of reagent grade, purchased from Sigma-Aldrich and used without further purification. All analytical-grade solvents were dried by standard procedures, distilled and deaerated before use. ^{1}H NMR spectra were recorded on a Varian Mercury-VX 300 spectrometer. The UV–Vis spectra were carried out on a UV–Vis Spectrophotometer (Shimadzu). The fluorescence spectra were performed on a PE LS55 fluorescence spectrometer. The chemical shifts were referenced to tetramethylsilane, TMS ($d = 0.00$). Mass spectra, reported as *m*/*z*, were obtained either on a Bruker Autoflex MALDI-TOF mass spectrometer or a Finnigan TSQ 710 (FAB-MS) mass spectrometer.

Synthesis of 4-(2-ethoxyethoxy)benzaldehyde (1)

To a 250 mL flask, 2-bromoethyl ether (37.62 g, 0.246 mol), 4-hydroxybenzaldehyde (32 g, 0.262 mol), anhydrous potassium carbonate (67.89 g, 0.491 mol) and 120 mL acetonitrile were added. The solution was heated to reflux for 24 h. Then, the solvent was evaporated in vacuo and the residue was dissolved in H_2O and extracted with ethyl acetate. The organic layers were washed with 2× 100 mL sodium hydroxide solution (1 N) and with 2× 100 mL saturated brine, respectively. The obtained solution was concentrated to get the pure product, yield 81%. ^{1}H NMR (400 MHz, $CDCl_3$) δ 9.72 (s, 1H, C<u>H</u>O), 7.68 (m, 2H, benzyl), 6.89 (m, 2H, benzyl), 4.05 (t, 2H, OC<u>H</u>$_2$CH$_2$O), 3.67 (t, 2H, OCH$_2$C<u>H</u>$_2$O), 3.45 (q, 2H, -C<u>H</u>$_2$CH$_3$), 1.09 (t, 3H, C<u>H</u>$_3$). Mass (ESI): calcd for $C_{11}H_{14}O_3$ $(M+H)^+$, 195.27; found 195.52.

Synthesis of carboxylic acid ester porphyrin (2)

To a 500-mL three-neck flask, methyl 4-formylbenzoate (7.12 g, 43 mmol), 4-(2-ethoxyethoxy)benzaldehyde (25.02 g, 129 mmol) and 260 mL propionic acid were added. The solution was stirred and heated to reflux. Subsequently, 11.34 g (169 mmol) freshly distilled pyrrole was added dropwise and the resulting solution was refluxed for another 2 h. The solvent was evaporated in vacuo and the residue was dissolved in CH_2Cl_2 and washed with saturated aqueous $NaHCO_3$ solution. The organic layer was then concentrated and the residue was subjected to silica chromatography (MeOH in CH_2Cl_2, 0–1% v/v), yield 5%. ^{1}H NMR (400 MHz, $CDCl_3$) δ 8.84 (s, 8H, β-pyrrole), 8.44 (d, 2H, CH), 8.32 (d, 2H, CH), 8.09 (d, 6H, CH), 7.27 (d, 6H, benzyl), 4.34 (d, 6H, OC<u>H</u>$_2$CH$_2$O), 4.11 (s, 3H, OC<u>H</u>$_3$), 3.94 (d, 6H, OCH$_2$C<u>H</u>$_2$O), 3.72 (q, 6H, –C<u>H</u>$_2$CH$_3$), 1.35(t, 6H, –CH$_2$C<u>H</u>$_3$), − 2.74 (s, 2H, N<u>H</u>). Mass (ESI): calcd for $C_{58}H_{56}N_4O_8$ $(M+H)^+$, 938.05; found 938.26.

Synthesis of carboxyl acid porphyrin (3)

The compound **2** (630 mg, 0.67 mmol) was dissolved in a mixture of 140-mL tetrahydrofuran and 140-mL 2-N KOH. After heating to reflux for 24 h, a portion of tetrahydrofuran and water was evaporated in vacuo. 1-N HCl was then added to adjust the pH of solution to neutral. The precipitate was isolated by centrifugation (3700 rpm, 5 min) and washed two times with water. The solid was dried under high vacuum (0.4 mbar) for a prolonged period to obtain 483-mg purple crystalline compound, yield 77%. ^{1}H NMR (400 MHz, DMSO-d_6) δ 8.88 (s, 8H, β-pyrrole), 8.37 (d, 2H, CH), 8.30 (d, 2H, CH), 8.12 (d, 6H, CH), 7.22 (d, 6H, benzyl), 4.36

(d, 6H, $OC\underline{H}_2CH_2O$), 3.91 (d, 6H, $OCH_2C\underline{H}_2O$), 3.75 (q, 6H, $-C\underline{H}_2CH_3$), 1.32(t, 6H, $-CH_2C\underline{H}_3$), − 2.88 (s, 2H, N<u>H</u>). Mass (ESI): calcd for $C_{57}H_{54}N_4O_8$ $(M+H)^+$, 924.06; found 924.50.

Synthesis of indomethacin-conjugated porphyrin (Por)

The compound **3** (483 mg, 0.523 mmol), Boc-protected 1,4-butanediamine (268.68 mg, 0.628 mmol), DMAP (128.5 mg, 1.052 mmol) and EDCI (201.7 mg, 1.052 mmol) were dissolved in 70-mL dichloromethane. The reaction mixture was stirred overnight under a nitrogen atmosphere. The solvent was evaporated in vacuo and the residue was subjected to silica chromatography (MeOH in CH_2Cl_2, 1–2% v/v) to get 246.9-mg product, yield 35%. ^{1}H NMR (400 MHz, $CDCl_3$) δ 8.75 (s, 8H, β-pyrrole), 8.12 (s, 2H, CH), 8.02 (d, 2H, CH), 7.89 (d, 6H, CH), 7.50 (d, 2H, p-chlorobenzoyl, H-3, H-5), 7.29 (d, 2H, p-chlorobenzoyl, H-2, H-6), 7.13 (m, 6H, benzyl), 6.73–6.84 (m, 3H, indolyl), 6.58 (m, 2H, $-N\underline{H}CH_2-$), 4.22 (d, 6H, $OC\underline{H}_2CH_2O$), 3.81 (d, 6H, $OCH_2C\underline{H}_2O$), 3.69 (s, 3H, $-OC\underline{H}_3$), 3.60 (q, 6H, $-C\underline{H}_2CH_3$), 3.5 (s, 2H, $-COC\underline{H}_2$), 3.44 (t, 2H, $-NHC\underline{H}_2-$), 3.22 (t, 2H, $-C\underline{H}_2NH-$), 2.29 (s, 3H, $C\underline{H}_3$), 1.53 (s, 4H, $-C\underline{H}_2C\underline{H}_2-$), 1.23 (t, 9H, $-CH_2C\underline{H}_3$), − 2.85 (s, 2H, N<u>H</u>). Mass (ESI): calcd for $C_{80}H_{78}ClN_7O_{10}$ $(M+H)^+$, 1333.97; found 1334.17.

Synthesis of zinc porphyrin complex (ZnPor)

The indomethacin-conjugated porphyrin (**Por**) (55 mg, 0.041 mmol) was dissolved in 10 mL dichloromethane and then heated to 40 °C, followed by addition of zinc acetate dihydrate (181.14 mg, 0.825 mmol) in 4-mL MeOH. The solution was refluxed for 3 h, and the completion of metal insertion was verified by UV–Vis spectroscopy and TLC. The solvent was evaporated in vacuo and the residue was subjected to silica column chromatography (40% hexane in CH_2Cl_2, v/v). The pure fractions were collected and concentrated under reduced pressure, which was then dissolved in a minimal amount of dichloromethane and precipitated in hexane to get 47-mg desired complex, yield 77%. ^{1}H NMR (400 MHz, $CDCl_3$) δ 8.81 (s, 8H, β-pyrrole), 8.16 (s, 2H, CH), 8.05 (d, 2H, CH), 7.94 (d, 6H, CH), 7.60 (d, 2H, p-chlorobenzoyl, H-3, H-5), 7.39 (d, 2H, p-chlorobenzoyl, H-2, H-6), 7.16 (m, 6H, benzyl), 6.79–6.94 (m, 3H, indolyl), 6.66 (m, 2H, $-N\underline{H}CH_2-$), 4.22 (d, 6H, $OC\underline{H}_2CH_2O$), 3.87 (d, 6H, $OCH_2C\underline{H}_2O$), 3.79 (s, 3H, $-OC\underline{H}_3$), 3.72 (q, 6H, $-C\underline{H}_2CH_3$), 3.67 (s, 2H, $-COC\underline{H}_2$), 3.52 (t, 2H, $-NHC\underline{H}_2-$), 3.33 (t, 2H, $-C\underline{H}_2NH-$), 2.40 (s, 3H, $C\underline{H}_3$), 1.63 (s, 4H, $-C\underline{H}_2C\underline{H}_2-$), 1.33 (t, 9H, $-CH_2C\underline{H}_3$). Mass (ESI): calcd for $C_{80}H_{76}ClN_7O_{10}Zn$ $(M+H)^+$, 1397.33; found 1397.57.

Synthesis of palladium porphyrin complex (PdPor)

The indomethacin-conjugated porphyrin (**Por**) (56 mg, 0.042 mmol) and palladium acetate (11.31 mg, 0.050 mmol) were dissolved in 10-mL dichloromethane and then heated to 70 °C. The completion of metal insertion was verified by UV–Vis spectroscopy and TLC. The solvent was evaporated in vacuo and the residue was washed with 3× 100 mL brine solution and 3× 100 mL H_2O, respectively. The organic layer was dried over Na_2SO_4 and evaporated in vacuo. The residue was purified by silica column chromatography (MeOH in CH_2Cl_2: 0–2% v/v) to get 50-mg product, yield 82%. ^{1}H NMR (400 MHz, $CDCl_3$) δ 8.81 (s, 8H, β-pyrrole), 8.16 (s, 2H, CH), 8.05 (d, 2H, CH), 7.94 (d, 6H, CH), 7.60 (d, 2H, p-chlorobenzoyl, H-3, H-5), 7.39 (d, 2H, p-chlorobenzoyl, H-2, H-6), 7.16 (m, 6H, benzyl), 6.79–6.94 (m, 3H, indolyl), 6.66 (m, 2H, $-N\underline{H}CH_2-$), 4.22 (d, 6H, $OC\underline{H}_2CH_2O$), 3.87(d, 6H, $OCH_2C\underline{H}_2O$), 3.79 (s, 3H, $-OC\underline{H}_3$), 3.72 (q, 6H, $-C\underline{H}_2CH_3$), 3.67 (s, 2H, $-COC\underline{H}_2$), 3.52 (t, 2H, $-NHC\underline{H}_2-$), 3.33 (t, 2H, $-C\underline{H}_2NH-$), 2.40 (s, 3H, $C\underline{H}_3$), 1.63 (s, 4H, $-C\underline{H}_2C\underline{H}_2-$), 1.33 (t, 9H, $-CH_2C\underline{H}_3$). Mass (ESI): calcd for $C_{80}H_{76}ClN_7O_{10}Pd$ $(M+H)^+$, 1436.44; found 1436.72.

Synthesis of platinum porphyrin complex (PtPor)

To a 10 mL flask, indomethacin-conjugated porphyrin (**Por**) (70 mg, 0.053 mmol), potassium tetrachloroplatinate (43.62 mg, 0.105 mmol), and 5 mL benzonitrile were added. The mixture was then heated to reflux for 48 h. The completion of metal insertion was verified by UV–Vis spectroscopy and TLC. The solvent was evaporated in vacuo and the residue was subjected to silica column chromatography (MeOH in CH_2Cl_2: 0–2% v/v). The pure fraction was collected and concentrated to give the product 46 mg, yield 78%. ^{1}H NMR (400 MHz, $CDCl_3$) δ 8.77 (s, 8H, β-pyrrole), 8.20 (s, 2H, CH), 8.11 (d, 2H, CH), 8.02 (d, $J = 8$ Hz, 6H, CH), 7.65 (d, 2H, p-chlorobenzoyl, H-3, H-5), 7.42 (d, 2H, p-chlorobenzoyl, H-2, H-6), 7.27 (m, 6H, benzyl), 6.69-6.95 (m, 3H, indolyl), 6.82 (m, 2H, $-N\underline{H}CH_2-$), 4.37 (d, 6H, $OC\underline{H}_2CH_2O$), 3.97 (d, 6H, $OCH_2C\underline{H}_2O$), 3.81 (s, 3H, $-OC\underline{H}_3$), 3.72 (q, 6H, $-C\underline{H}_2CH_3$), 3.69 (s, 2H, $-COC\underline{H}_2$), 3.56 (t, 2H, $-NHC\underline{H}_2-$), 3.36 (t, 2H, $-C\underline{H}_2NH-$), 2.43 (s, 3H, $C\underline{H}_3$), 1.61 (s, 4H, $-C\underline{H}_2C\underline{H}_2-$), 1.35 (t, 9H, $-CH_2C\underline{H}_3$). Mass (ESI): calcd for $C_{80}H_{76}ClN_7O_{10}Pt$ $(M+H)^+$, 1525.50; found 1525.83.

UV–Vis absorption and fluorescence spectra

The UV–Vis absorption spectrum and fluorescence spectrum of four porphyrin conjugates were measured in DMSO solution.

Singlet oxygen detection

Firstly, DCFH-DA was treated by 0.1-M NaOH for 30 min to convert into dichlorofluorescin. Irradiation of activated DCFH solutions in the presence of photosensitizer solutions (1×10^{-6} M in PBS buffer with 0.5% DMSO) results in the transformation of non-fluorescent activated into highly fluorescent 2′,7′-dichlorofluorescein with emission peak at 532 nm. The mixed solutions were exposed to light irradiation (xenon lamp, 50 W) for different time intervals. The fluorescence spectra of DCFH solutions were recorded in 500–580-nm emission range under an excitation of 488 nm. The PBS buffer was used as control.

Cell viability assays

Human cervical carcinoma (HeLa) cells were cultured in DMEM (Dulbecco's Modified Eagle's Medium) supplemented with 5% FCS (Fetal Calf Serum), 100 U/mL penicillin, 100 µg/mL streptomycin at 37 °C and 6% CO_2. The MTT viability assay was performed according to a standard method. In brief, HeLa cells (3×10^3/well) were seeded in 96-well plates for 24 h prior to exposure to drugs. The cells were treated with samples overnight in the dark. The cytotoxicity was determined by the MTT reduction assay. The cell monolayers were rinsed twice with phosphate-buffered saline (PBS) and then incubated with 50-µL MTT solution (0.5 mg/mL) at 37 °C for 3 h. After the media was removed, 100 µL of DMSO was added. The solution was shook for 30 min to dissolve the formed formazan crystals in living cells. The absorbance was measured at dual wavelength, 540 nm and 690 nm, on a Labsystem Multiskan microplate reader (Merck Eurolab, Switzerland). Each dosed concentration was performed in triplicate wells, and repeated twice for the MTT assay.

The photocytotoxicity of samples was assessed by a similar protocol. In general, HeLa cells (3×10^3/well) were incubated in 96-well plates for 24 h prior to exposure to drugs. The cells were treated with samples in the dark overnight. Afterwards, the cell was exposed to yellow light (4 J/cm^2) produced from a 400-W tungsten lamp fitted with a heat-isolation filter and a 500-nm long-pass filter. The fluence rate was 6 mW/cm^2. Cell viability was determined by the MTT reduction assay.

Confocal laser scanning microscope studies

HeLa Cells were cultured in RPMI 1640 Medium (Gibco^{Tm}) containing 10% fetal bovine serum and 1% antibiotics penicillin and streptomycin (P/S) and incubated at 37 °C in a humidified 5% CO_2 atmosphere. Cells (6×10^3 cells per well) were seeded in 6-well plates (a sterile cover slip was put in each well) and incubated 2 days at 37 °C in a humidified 5% CO_2 atmosphere. After refreshed with new medium, the cells were incubated with photosensitizers at a concentration of 1.0 µM for 12 h at 37 °C in the. After that, the supernatant was carefully removed and the cells were washed three times with PBS. Subsequently, the slides were mounted and observed by confocal microscope (Zeiss Laser Scanning Confocal Microscope; LSM7 DUO) and then the data was analyzed using ZEN 2009 software (Carl Zeiss).

For co-staining of porphyrin and LysoTracker® Green DND-26: HeLa cells were first incubated with porphyrin at 37 °C for 12 h, then further incubated with LysoTracker® Green DND-26 (10 µg/mL) for 10 min at 37 °C. Before imaging on the confocal microscope, the cells were washed with PBS three times.

Results and discussion

Synthesis

The synthesis of indomethacin–porphyrin conjugate and its metal complexes was demonstrated in Scheme 1. Firstly, stoichiometric pyrrole was condensed with methyl 4-formylbenzoate and 4-(2-ethoxyethoxy) benzaldehyde to yield 5,10,15-tri-(4-(2-ethoxyethoxy))-20-(4-methyl-phenyl) porphyrin. 1,4-butanediamine was mono-protected by BOC anhydride and the indomethacin derivative (INDO-NH_2) was synthesized following the procedure described in the literature [20]. The carboxylic acid ester group in porphyrin (**2**) was hydrolyzed by a base-catalyzed reaction, affording 5,10,15-tri-(4-(2-ethoxyethoxy))-20-(4-carboxyphenyl) porphyrin (**3**) in 75% yield. Then, the indomethacin terminated with amine was coupled with porphyrin **3** in the presence of DMAP and EDCI to yield indomethacin–porphyrin conjugate. Finally, the porphyrin conjugate was coordinated with related metal salts to obtain the corresponding metal porphyrin complexes.

Photophysical properties

The photophysical properties of porphyrin–indomethacin conjugate and its metal complexes were studied in DMSO solution. The UV–Vis absorption spectrum of free base porphyrin conjugate exhibited a sharp Soret band centered at 422 nm and weak Q bands at 519, 555, 593 and 651 nm, respectively. After metal insertion, the two peaks in the Q bands of free base porphyrin disappeared, as shown in Fig. 1a, due to the increase of molecular symmetry. The fluorescence emission of porphyrin–indomethacin conjugate and its metal complexes was tested in DMSO solution. As shown in Fig. 1b, the palladium and platinum porphyrin complexes (PdPor and PtPor) did not show any significant fluorescence, while free base porphyrin and zinc porphyrin complex

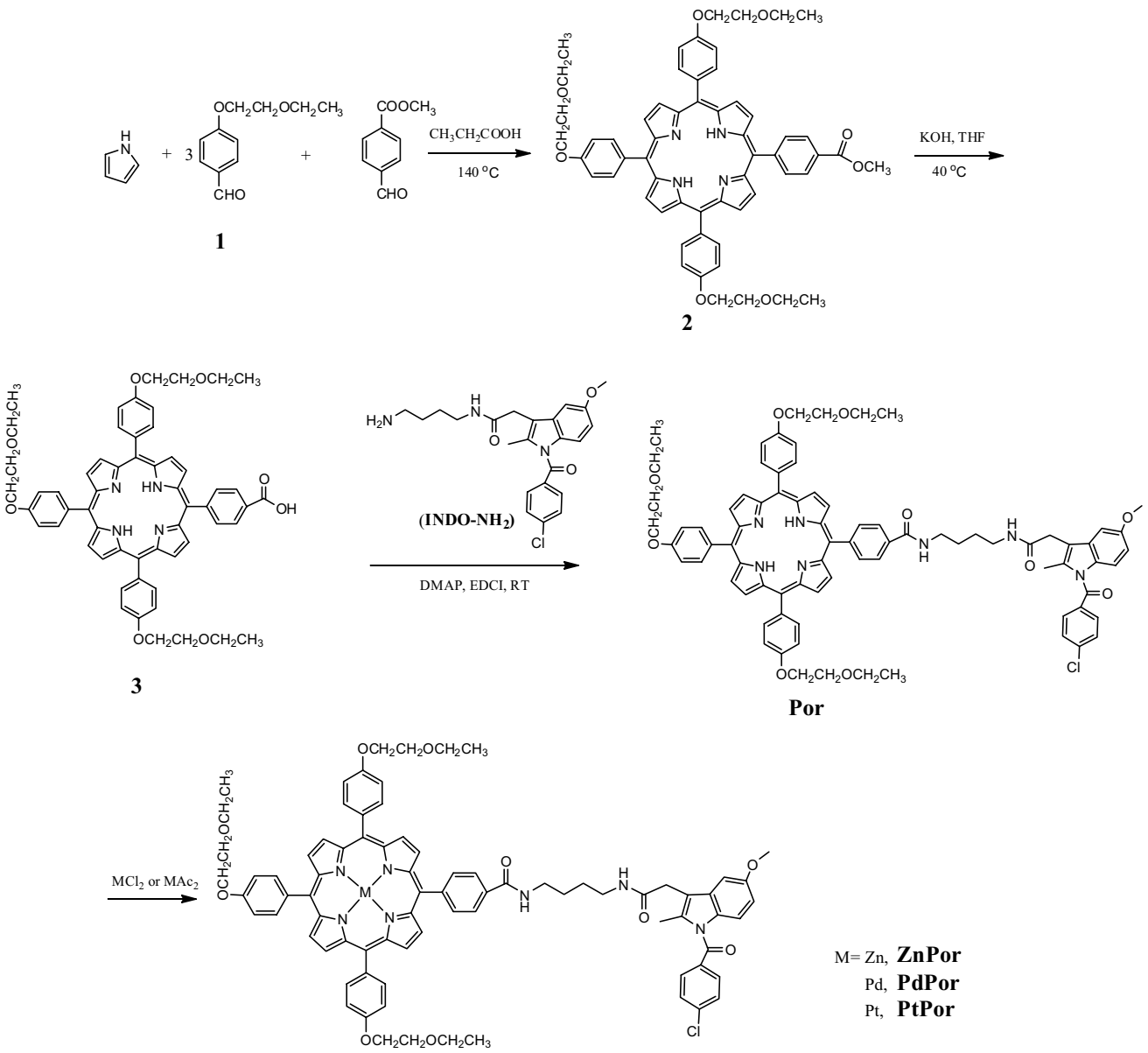

Scheme 1 Synthetic routes of Por, ZnPor, PdPor, and PtPor

exhibited intense red emission, with maximum peak around at 673 and 622 nm, respectively. The excitation spectra in Fig. 1b indicated that both the two compounds displayed the similar excitation bands with maximum around at 400 nm.

Singlet oxygen detection

The singlet oxygen generation of photosensitizers was investigated by a reactive oxygen species (ROS) probe 2′, 7′-dichlorofluorescin diacetate (DCFH-DA). Firstly, DCFH-DA was treated with NaOH solution to transfer to DCFH before being used in vitro. The non-fluorescent DCFH will be rapidly oxidized to a green fluorescent DCF in the presence of reactive oxygen species. The green fluorescence (λ_{em} = 532 nm) of DCFH will increase quantitatively upon reacting with ROS generated from photosensitizers. As shown in Fig. 2, the fluorescence intensity of DCFH displays a time-dependent enhancement upon reaction with ROS, generated from porphyrins when irradiated with a xenon lamp. Under the same conditions, the fluorescence intensity of DCFH mixed with platinum porphyrin complex was enhanced over two hundreds times after irradiation for 8 min, which is apparently higher than that of free base porphyrin and other metal porphyrin complexes, suggesting that PtPor had the highest singlet oxygen quantum yield. Since the capacity of photosensitizer to generate $^1O_2$ is dependent

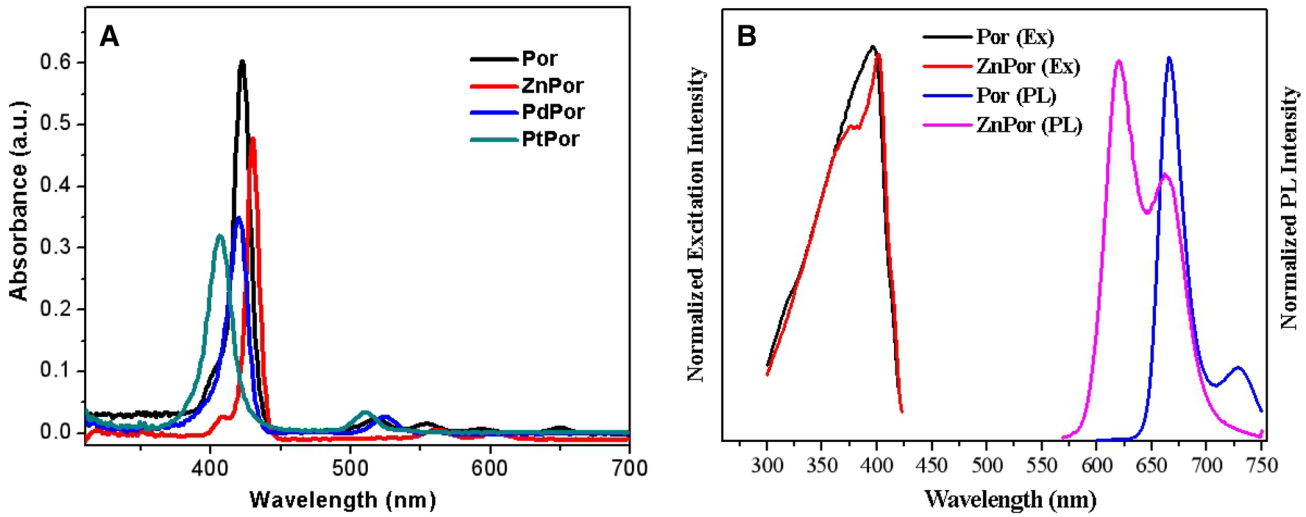

Fig. 1 **a** UV–Vis absorption spectrum, **b** emission and excitation spectrum of Por, ZnPor, PdPor, and PtPor

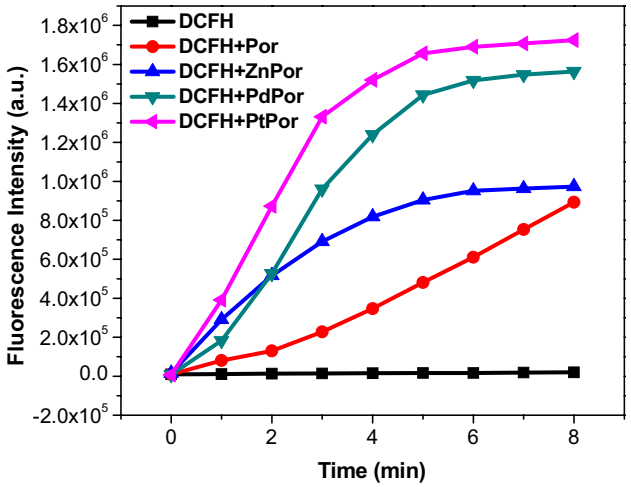

Fig. 2 The changes of fluorescence intensity at the characteristic peak of DCFH (525 nm) as a function of irradiation time

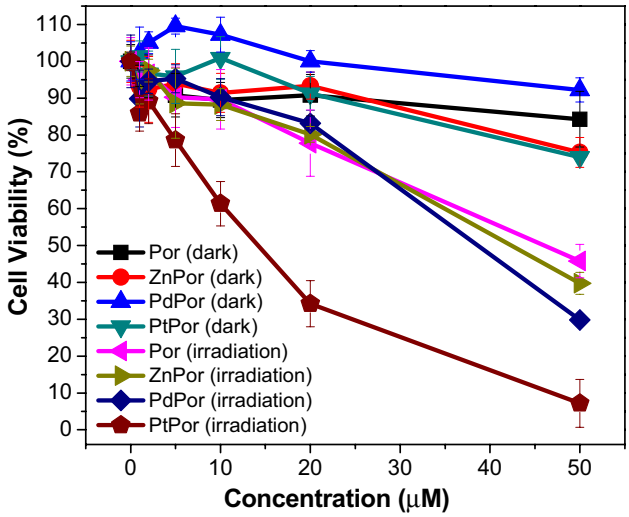

Fig. 3 Concentration dependence of the cytotoxicity of Por, ZnPor, PdPor, and PtPor against HeLa cells, as determined by a MTT assay. Data represent the mean values from three independent experiments. Error bars are standard deviations

on the efficiency of the intersystem crossing (ISC) from ^{1}PS* to ^{3}PS*, the higher singlet oxygen quantum yield of PtPor is probably due to the heavy-atom effect of platinated porphyrin.

In vitro dark cytotoxicity and photocytotoxicity

To verify the cytotoxic effects of the synthesized porphyrins, a MTT assay was performed against HeLa cells. As shown in Fig. 3, free base porphyrin and its metal complexes all exhibited the low dark toxicity after 24-h incubation with HeLa cells in a dose-dependent manner. When the concentration of porphyirns was less than 20 μM, they did not lead to any significant decrease in survival fraction, with cell viability higher than 90%. The photocytotoxicity of synthesized porphyrins was evaluated by a similar protocol. As shown in Fig. 3, after irradiation, the cell survival fraction decreased significantly as the concentration of porphyrins increased from 0 to 50 μM, indicating that the cell death was only triggered by a combination of the PSs and light. Besides, the PtPor showed the stronger photocytotoxicity to tumor cells than that of other porphyrin–indomethacin conjugates, which is consistent with the trend of singlet oxygen yield of these photosensitizers. The cell viabilities of PtPor at 50 μM were determined to

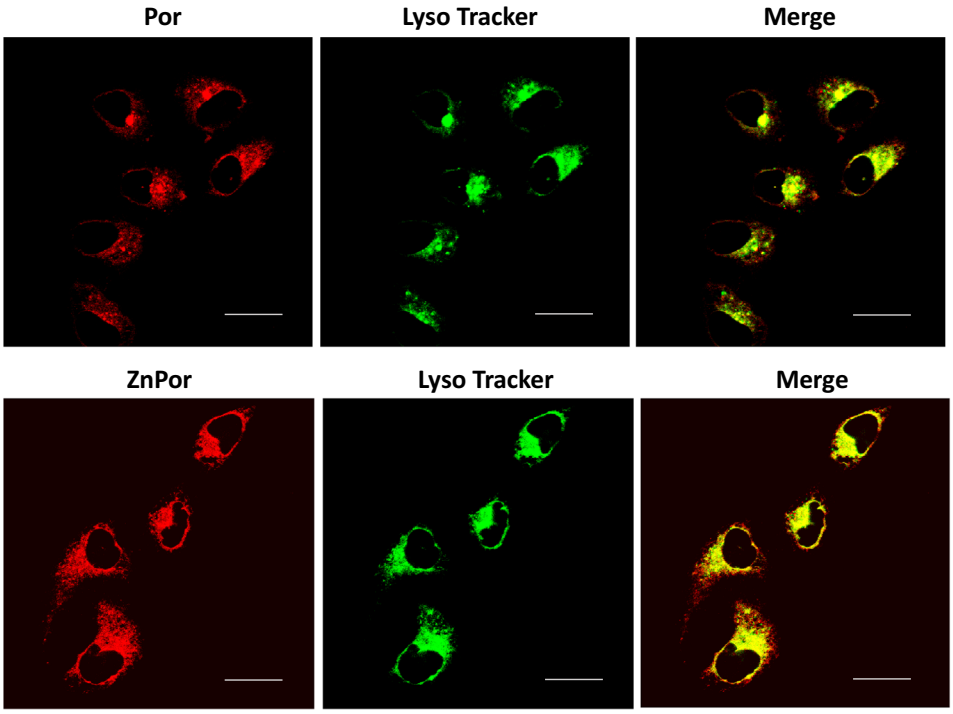

Fig. 4 Laser scanning confocal microscopy images (λ_{ex} = 405 nm) of HeLa cells incubated with Por and ZnPor at a concentration of 2 μM in the cell culture medium for 8 h. The lysosomes (green) were stained with LysoTracker® Green DND-26 (50 μM). (The scale bar is 20 μm)

be only 7.6% upon irradiation, indicating it is an efficient antitumor agent for cancer in PDT.

To evaluate the role of indomethacin, we synthesized a platinum porphyrin complex without conjugation of indomethacin (PtPor1) for comparison. As shown in Fig. S1A, the PtPor and PtPor1 showed the similar singlet oxygen quantum yield under the same condition, indicating that indomethacin did not affect the generation of singlet oxygen. Moreover, the cytotoxic effects of PtPor and PtPor1 against HeLa cells were also evaluated and compared under the dark and irradiation condition. As shown in Fig. S1B, PtPor exhibited a little higher dark toxicity related to PtPor1 at the concentration of 50 μM, which was probably due to the indomethacin alone had antitumour activity to some extent, as reported in previous literature [17]. Besides, the PtPor showed the stronger photocytotoxicity to tumor cells than that of free platinum porphyrin without indomethacin (PtPor1) at the same condition. Since the two compounds showed the similar singlet oxygen quantum yield, the higher PDT efficiency of PtPor was probably assigned to the enhanced accumulation of photosensitizer in tumor cells in the role of indomethacin [20].

Confocal fluorescence imaging

Since the free base porphyrin and zinc porphyrin complex exhibited significant emission in the visible region, the cellular uptake and subcellular localization of these two compounds were confirmed by fluorescence confocal laser microscopy. As shown in Fig. 4, after incubation of HeLa cells with 2 μM Por and ZnPor for 8 h, intense red fluorescence was observed in the cytoplasm, indicating the accumulation of porphyrins in cancer cells. To further figure out the localization of Por and ZnPor in HeLa cells, LysoTracker Green DND-26 staining was applied to visualize the cell lysosomes. As shown in Fig. 4, the red emission from Por or ZnPor is almost overlapped with that of green fluorescence of DND-26, indicating the photosensitizers are primarily localized in the lysosomes of cells.

Conclusion

In this study, a series of metalloporphyrin–indomethacin conjugates tethered with poly(ethylene glycol) (PEG) chains were synthesized and characterized. The metal porphyrin complexes exhibited the higher singlet oxygen quantum yield than that of free base porphyrin, probably due to the heavy atom effect. The order of $^1O_2$ yield of the synthesized porphyrins was PtPor > PdPor > ZnPor > Por. The MTT assay against HeLa cells verified the low cytotoxicity of porphyrin–indomethacin conjugates in the dark. Upon irradiation, the platinated porphyrin (PtPor) showed the highest therapeutic activity against HeLa cells among these photosensitiers, ascribed to its high efficiency of $^1O_2$ generation. The cellular uptake and subcellular localization of the porphyrin–indomethacin conjugates were further evaluated through a confocal laser scanning microscope. The results

showed that the conjugates were primarily localized in the lysosomes of cells. An investigation into the application of these novel porphyrins as selective anticancer photodynamic therapeutic agents is currently underway.

Acknowledgements The work was supported by the National Natural Science Foundation of China (NSFC) (21601142, 81503036) and the Natural Science Foundation of Hubei Province (2017CFB689).

References

1. Zhu S, Yao S, Wu F, Jiang L, Wong KL, Zhou J, Wang K (2017) Platinated porphyrin as a new organelle and nucleus dual-targeted photosensitizer for photodynamic therapy. Org Biomol Chem 15:5764–5771
2. Wu F, Chen J, Li Z, Su H, Leung KCF, Wang H, Zhu X (2018) Red/near-infrared emissive metalloporphyrin-based nanodots for magnetic resonance imaging-guided photodynamic therapy in vivo. Part Part Syst Charact 35:1800208
3. Xu Z, Yu F, Wu F, Zhang H, Wang K, Zhang X (2015) Synthesis, DNA photocleavage, singlet oxygen photogeneration and two photon absorption properties of ruthenium-phenanthroline porphyrins. J Porphyr Phthalocya 19:1–7
4. Berg K, Golab J, Korbelik M, Russell D (2011) Drug delivery technologies and immunological aspects of photodynamic therapy. Photoch Photobio Sci 10:647–648
5. Lovell JF, Liu TW, Chen J, Zheng G (2010) Activatable photosensitizers for imaging and therapy. Chem Rev 110:2839–2857
6. Ethirajan M, Chen Y, Joshi P, Pandey RK (2011) The role of porphyrin chemistry in tumor imaging and photodynamic therapy. Chem Soc Rev 40:340–362
7. Zhu S, Wu F, Wang K, Zheng Y, Li Z, Zhang X, Wong WK (2015) Photocytotoxicity, cellular uptake and subcellular localization of amidinophenylporphyrins as potential photodynamic therapeutic agents: an in vitro cell study. Bioorg Med Chem Lett 25:4513–4517
8. Zheng Y, Zhu S, Jiang L, Wu F, Huang C, Li Z, Wong KL, Xu Z, Wang K (2017) Synthesis, singlet oxygen generation, photocytotoxicity and subcellular localization of azobisporphyrins as potentially photodynamic therapeutic agents in vitro cell study. J Porphyr Phthalocya 21:122–127
9. Yao S, Zheng Y, Jiang L, Xie C, Wu F, Huang C, Zhang X, Wong KL, Li Z, Wang K (2018) Methylene violet 3RAX-conjugated porphyrin for photodynamic therapy: synthesis, DNA photocleavage, and cell study. RSC Adv 8:4472–4477
10. Hayashi K, Nakamura M, Miki H, Ozaki S, Abe M, Matsumoto T, Ishimura K (2014) Photostable iodinated silica/porphyrin hybrid nanoparticles with heavy-atom effect for wide-field photodynamic/photothermal therapy using single light source. Adv Funct Mater 24:503–513
11. Harris JM, Chess RB (2003) Effect of pegylation on pharmaceuticals. Nat Rev Drug Discov 2:214–221
12. Nawalany K, Rusin A, Kepczynski M, Filipczak P, Kumorek M, Kozik B, Nowakowska M (2012) Novel nanostructural photosensitizers for photodynamic therapy: in vitro studies. Int J Pharmaceut 430:129–140
13. Huang H, Wang D, Zhang Y, Zhou Y, Geng J, Chitgupi U, Cook TR, Xia J, Lovell JF (2016) Axial PEGylation of tin octabutoxy naphthalocyanine extends blood circulation for photoacoustic vascular imaging. Bioconjugate Chem 27:1574–1578
14. Wu F, Su H, Cai Y, Wong WK, Jiang W, Zhu X (2018) Porphyrin-implanted carbon nanodots for photoacoustic imaging and in vivo breast cancer ablation. ACS Appl Bio Mater 1:110–117
15. Brunelli C, Amici C, Angelini M, Fracassi C, Belardo G, Santoro MG (2012) The non-steroidal anti-inflammatory drug indomethacin activates the eIF2α kinase PKR, causing a translational block in human colorectal cancer cells. Biochem J 443:379–386
16. Yang K, Zhang X, Yang F, Wu F, Zhang X, Wang K (2017) DNA photocleavage and binding modes of methylene violet 3RAX and its derivatives: effect of functional groups. Aust J Chem 70:830–836
17. Han L, Peng B, Ma Q, Ma J, Li J, Li W, Laporte K (2013) Indometacin ameliorates high glucose-induced proliferation and invasion via modulation of e-cadherin in pancreatic cancer cells. Curr Med Chem 20:4142–4152
18. Marydasan B, Nair AK, Ramaiah D (2013) Optimization of triplet excited state and singlet oxygen quantum yields of picolylamine-porphyrin conjugates through zinc insertion. J Phys Chem B 117:13515–13522
19. Mathai S, Smith TA, Ghiggino KP (2007) Singlet oxygen quantum yields of potential porphyrin-based photosensitisers for photodynamic therapy. Photochem Photobio Sci 6:995–1002
20. Uddin MJ, Crews BC, Blobaum AL, Kingsley PJ, Gorden DL, McIntyre JO, Matrisian LM, Subbaramaiah K, Dannenberg AJ, Piston DW, Marnett LJ (2010) Selective visualization of cyclooxygenase-2 in inflammation and cancer by targeted fluorescent imaging agents. Cancer Res 70:3618–3627